

THE EFFECTS OF 3D PRINTED MOLDS ON METAL CASTINGS

Dean Snelling¹, Heather Blount², Charles Forman², Kelly Ramsburg², Andrew Wentzel²,
Christopher Williams¹, Alan Druschitz²

¹ Design, Research, and Education for Additive Manufacturing Systems Laboratory; Department
of Mechanical Engineering

² Department of Material Science
Virginia Tech, Blacksburg, VA

ABSTRACT

Additive manufacture of sand molds via binder jetting enables the casting of complex metal geometries. Various material systems have been created for 3D printing of sand molds; however, a formal study of the materials' effects on cast products has not yet been conducted. In this paper the authors investigate potential differences in material properties (microstructure, porosity, mechanical strength) of A356 – T6 castings resulting from two different commercially available 3D printing media. In addition, the material properties of cast products from traditional “no-bake” silica sand is used as a basis for comparison of castings produced by the 3D printed molds.

Keywords: Binder Jetting, Indirect 3D Printing, Metal Casting, Sand Casting

1. EFFECTS OF MOLDING MATERIALS ON CASTINGS

1.1. Additive Manufacturing of Sand Molds for Metal Casting

Additive Manufacturing (AM) has enabled the direct production of molds without the need for a pattern. Specifically, the binder jetting 3D Printing (3DP) process has been used to directly fabricate sand molds and core boxes by selectively jetting binder into a powder bed of foundry sand [1].

A schematic of the binder jetting process is provided in Figure 1. During binder jetting, a polymer binder is printed onto a bed of powder using a traditional inkjet print head to form one cross-sectional layer of the part. After a layer of binder is printed, the powder bed lowers, and fresh powder is spread over the powder bed using a roller. Then, the next layer of the part is patterned onto the powder bed atop the previous layer. In this manner, the object is constructed layer by layer.

After the mold is printed, the excess powder is removed using compressed air or vacuum. Often, the printed molds are then cured in an oven to eliminate a portion of the binder (Figure 2a). The printed part can also be used as a core or as a complete mold, which includes runners, gates, and a down-sprue (Figure 2b) [2]. Molten metal is then cast into the mold to create the

casting (Figure 2c). 3DP of molds for metal casting has been commercialized by a variety of companies, including 3D Systems [3], ExOne [4], and Viridis3D [5].

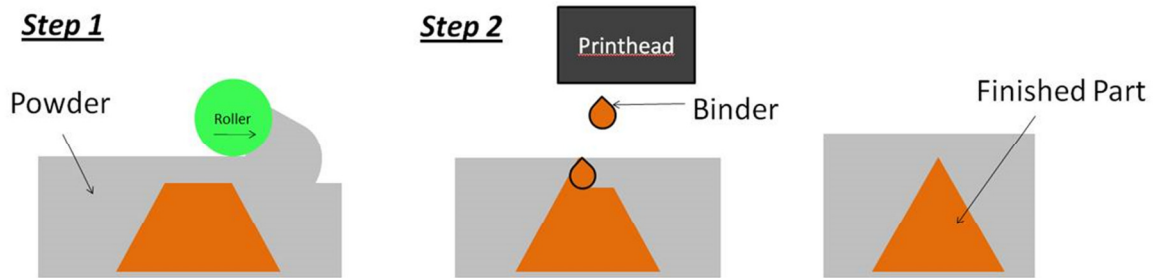


Figure 1. Schematic of the binder jetting process

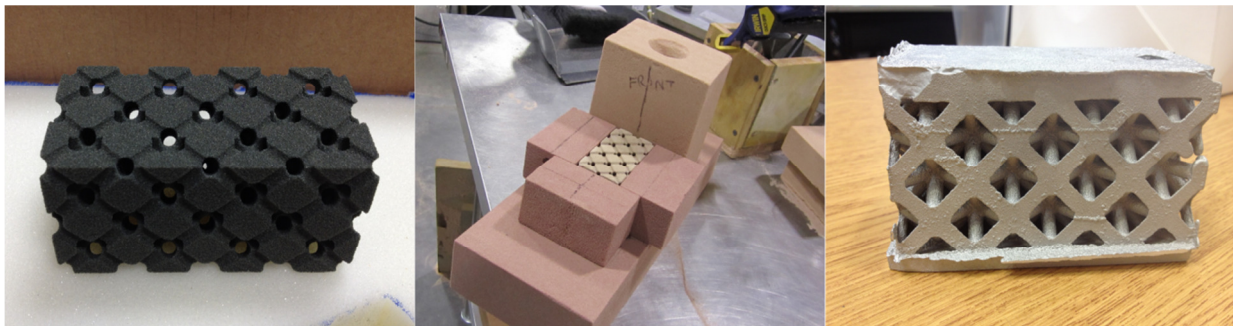


Figure 2. a) Complex printed mold created using binder jetting, b) no-bake outer mold, and c) cast complex structure

Many of the applications for additively manufactured sand molds are in providing a means to offer flexible tooling for traditionally designed castings. However, an important asset of the process is that the geometric freedoms offered by AM can be leveraged to provide a means for metal casting of complex geometries that are not possible to fabricate via traditional casting means [6]. In addition, the layer-by-layer process of fabricating sand molds enables a designer to uniquely integrate vents, sprues, runners directly into the mold design. Finally, as the final part is created outside of the AM systems' build chamber, the binder jetting and casting process chain enables the creation of large metal geometries. Specifically, multiple molds may be printed and fitted together with core paste to pour large metal castings.

1.2. Traditional Molding Material Effects on Castings

Although AM of sand molds has enabled designers to overcome manufacturing restrictions, little is known about the materials systems' effects on metal castings. This gap in knowledge is contradictory to the knowledge base in traditional sand casting. Many of the common aggregates used for the formation of molds in traditional sand casting are comprised of silica sand, natural minerals, synthetics, and other particulate materials [7]; each component with differing characteristics such as composition, grain size, and binder or compaction requirement. As a result, the properties of subsequent metal castings vary due to their reaction to the mold. For example, the quality of a casting can change due to water vapor stored in the mold, free

hydrogen, and organics as the metal flows and solidifies [7]. These reactions inherently affect the final cast product and can produce defects such as porosity, oxidation, carbon formation, and surface roughness [7].

1.3. Prior Research in 3DP of Sand Molds

This existing understanding of sand molds on metal casting cannot be directly applied to AM sand materials systems as they are the working materials are dissimilar. There is limited literature that explores the effects of 3D printable mold material on castings. Instead, most of prior research is focused in studying the molds produced by ZCast® [8–10]. For example, McKenna et al. performed tests on ZCast®, to determine the effects of temperature and curing time on permeability and compressive strength of the mold. A mathematical model was used to determine an optimal curing time and temperature for both permeability and compressive strength [11]. In previous work, the authors investigated the binder content of ZCast® material system and found it had a significantly higher binder content (up to 8% binder) than traditional no-bake foundry sand [2]. The higher binder content of the ZCast® printed molds causes molds to generate more gas during casting, which can cause defects in the final parts [2]. A new curing cycle with higher temperatures for a shorter duration produced more consistent cast structures with fewer gas defects [2]. In addition, Gill & Kaplas compared castings printed with ZCast® and Investment casting using starch and plaster, including dimensional tolerances, hardness values, surface roughness, production cost, and shrinkage [12]. Experiments were also run at different shell thicknesses. It was determined that starch based investment casting produced higher hardness values and slightly better surface roughness, where ZCast produced better dimensional tolerances all from a recommended shell thickness range of 12-2mm [12]. It was also concluded there is optimal settings in terms of time and shell thickness to minimize cost based on individual builds [12].

1.4. Overview of Work

In order to ensure quality cast parts, the effects of final cast material properties needs to be studied using different molding materials. The primary goal of this work is to compare two commercially available 3D printing 3DP powders: ViriCast™ (produced by Viridis3D^a) and ZCast® (produced by 3D Systems^b). Additionally, this work compares these two 3DP powders on the basis of the handleability of the resultant printed molds and the properties of the cast metal parts they produce. The 3DP powders will also be compared to traditional no-bake foundry sand in order to determine whether 3D printed molds can produce metal parts of comparable quality to traditional casting approaches.

An explanation of multiple tests utilized to characterize both 3DP sands and no-bake sand and material properties will be presented in Section 2. These tests include sieve analysis, tensile testing, surface roughness, density, hardness, porosity, microstructure, and compression tests. The results of these tests are presented and statistically analyzed in Section 3 Finally, in conclusion, an overview and future work is given in Section 4.

^a <http://www.viridis3d.com/metalcasting.htm>

^b <http://www.zcorp.com/en/Products/3D-Printers/Spectrum-Z510/spage.aspx>

2. EXPERIMENTAL PROCEDURE

2.1. Characterization of 3D Printing Powder

Functionally, the two sands investigated in this paper are similar. They are both processed via a binder jetting AM process, and are both designed for receiving molten metal for sand casting applications. The only stated performance difference is in their maximum casting temperatures: ViriCast™ can be cast at 2650°F (1454.4 °C) and can be used to cast ferrous and non-ferrous alloys; ZCast® has a maximum cast temperature at 2000°F (1093.3 °C) and can only be used for casting non-ferrous alloys. Further differences between the two powders are identified by further characterization experiments, including sieve analysis and tensile testing of cured sand samples.

Sieve Analysis

Standard sieve tests according to AFS 1105-00-S [13] and AFS 1106-00-S [13] were previously performed on ZCast® powder and no-bake sand to determine particle size distribution [2]. A sieve test was performed on the ViriCast™ powder following the same standard procedure.

Tensile Testing

The mechanical strength of the molds was characterized via tensile testing. Tensile testing was previously performed on ZCast® powder and no-bake foundry sand according to AFS 3342-00-S to determine handleability of the material [2]. Five equivalent dog-bone shaped specimens were printed using a 3D Systems Spectrum Z510 3D printer with ViriCast™ powder and 3D Systems zb56 binder; the dog-bones were then cured at 400 °F (204.4 °C) for five hours [2]. Tensile testing was performed using a tensile testing machine to determine the mold fracture strength. Collected data and modes of fracture for ViriCast™ molds were compared with ZCast®, as well as no-bake foundry sand molds.

2.2. Characterization of Cast A356 Cylinders

The primary goal of this research was to compare the properties of metal cast in (i) ViriCast™ molds, (ii) ZCast® molds, and (iii) no-bake foundry sand molds. The two 3D printed sands are treated as the experimental group; chemically bonded silica sand, also known as no-bake sand, is treated as the control, since there exists published information about its casting properties [14]. The binder ratio in the no-bake sand was 4:1 of Phenoset RB to APR-015 hardener/catalyst, which accounted for approximately 1.6% of the sand mixture [2]. A Palmer M50XLD continuous sand mixer was used to mix the silica sand and binder to create the no-bake sand [2].

To make the 3DP molds, hollow cylinders (inner diameter one inch, wall thickness of 1 inch, and length of 4 inches) were designed using CAD. This specific inner diameter was chosen given the ability to machine to typical specimen sizes for ASTM compression tests given in ASTM E9-09 [15]. Six cylindrical molds were then printed in both ViriCast™ and ZCast® powders at their individual manufacturer's process parameter specifications (Table 1). The printed mold can is illustrated in Figure 3a and the manufacturer's process parameters in Table 1.

The resultant printed molds were then post-processed according to their manufacturer’s specifications: ViriCast™ molds were cured at 400°F (204.4°C) for five hours, and ZCast® molds were cured at 600 °F (316 °C) for one hour. Then, no-bake foundry sand was used to create the down-sprue, runners and gates. In order to create the no-bake molds, one inch diameter dowel rods were used to create four cylindrical molds in no-bake foundry sand.

Table 1. 3D Printed mold material manufacturer process parameter specifications

3D Printed Material		Saturation Level	Binder/Volume Ratio
ZCast®	Shell	94%	0.204517
	Core	49%	0.0530748
ViriCast™	Shell	85%	0.184935
	Core	120%	0.129979

A356 alloy was cast into all the molds. A standard T6 heat treatment of 1005°F (540.6 °C) for six hours and artificial aging at 315°F (157.2 °C) for five hours was applied to the cylinders. The cylinders were cut into top, middle, and bottom sections for material analysis as shown in Figure 3b.

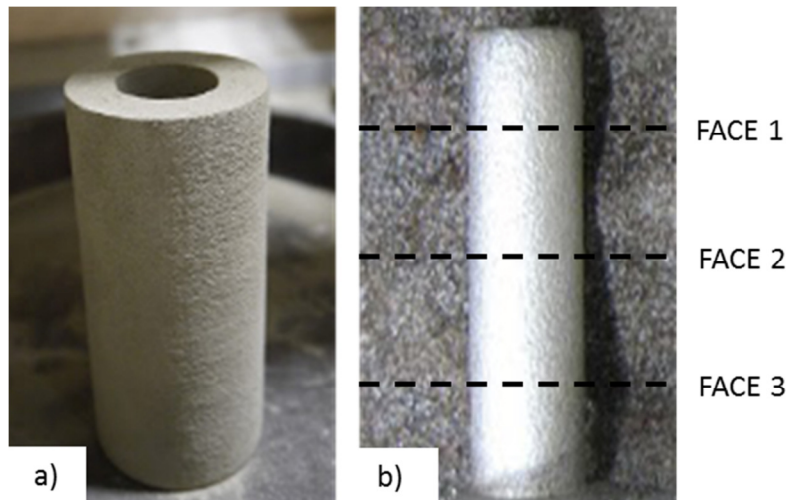


Figure 3. a) 3D printed cylindrical mold and b) cast cylinder with diagram of cylinder sections

Two top sections, two middle sections, and two bottom sections of the cylinders cast from each mold material were analyzed for surface roughness, density, hardness, porosity, and microstructure. The remaining specimens were machined for compression testing. Average values for the overall cylinders are presented along with standard deviation to aid analysis.

Surface Roughness

Surface roughness was measured using a Phase II SRG Surface Roughness Tester. Roughness average (R_a) of the cylinders cast using different molds was measured.

Density

Archimedes' Principle was used to determine the density of the cast A356 aluminum cylinders created by each of the mold types. Three trials were conducted for each cylinder section.

Hardness

Samples were mounted in PhenoCure® Resin Powder and burnished to with 240, 320, 400, and 600 grit polishing paper using the Ecomet® 3 Variable Speed Grinder-Polisher. Hardness testing was performed using a LECO Vickers Hardness Tester LV700AT. The cross-section hardness was measured in five locations of each cylinder.

Porosity

The sample surfaces were ground to remove indentations from hardness testing, and then re-polished using 240, 320, 400, and 600 grit polishing paper. Polishing was conducted using 5 μm and 1 μm alumina suspensions and a final finishing cloth. Final polishing was conducted with 0.04 μm colloidal silica and a final finishing cloth. Nine optical micrographs were taken of each sample for porosity measurements. ImageJ software was used to find the percent porosity by calculating the percentage of the total area covered by pores in each micrograph [16]. To accomplish this, the software was used to adjust the threshold of the image, highlight the pores, and measure the percent area of the pores. The threshold color brightness was adjusted until the pores were fully highlighted, and the size settings for analyzing particles were adjusted until the software recognized the pores. The ImageJ settings depended on the original saturation and contrast of the images. For example, micrographs with less contrast between black pores and surrounding material require higher threshold color brightness settings in ImageJ to fully highlight pores. Table 2 shows the ImageJ settings used to calculate porosity.

Table 2. ImageJ settings for calculating porosity of aluminum cylinders

Mold Material	Threshold: Color Brightness	Analyze Particles: Size
3DP Powders	28	115-Infinity
No-Bake	95	15-Infinity

Microstructure

Next, the microstructure of the aluminum samples were revealed by etching with Weck's reagent [17], [18], which contains 100 mL water, 4 g KMnO_4 , and 1 g NaOH . The sample surfaces were submerged in Weck's reagent [17], [18] and agitated for 20 seconds. After rinsing with water and alcohol, the samples were blown dry. Optical microscopy was performed to characterize the microstructure and determine the dendrite arm spacing in each sample.

Compression Testing

Compression specimens were machined to a diameter of $\frac{1}{2}$ in. and length of 1 in. according to ASTM standard E9-09 [15]. Compression tests were conducted using an MTS Insight Electromechanical 150 kN Standard Length Testing System to measure the compressive yield strength. The strain rate was fixed at 0.005 in./min. Compressive yield strengths were found using a 0.02% offset from the elastic region of the stress-strain curve. Compression tests were not performed on the cylinders cast using no-bake foundry sand since the compression behavior cast T6-A356 aluminum is published information [14].

3. RESULTS AND DISCUSSION

3.1. Properties of 3D Printing Powder

Sieve Analysis

Previous testing revealed that the no-bake sand had an AFS grain fineness number (GFN) of 57, while the ZCast® powder had an AFS GFN of 143 [2]. The results of the sieve analysis from silica sand and ZCast® are seen in Table 3 and ViriCast™ in Table 4.

Table 3. Sieve analysis and AFS grain fineness number for silica sand and ZCast® powder [2]

	Silica Sand	3DP Sand
Seive Size	Percent Retained	Percent Retained
12	0.00	0.00
20	0.00	0.00
30	0.00	0.00
40	1.34	0.00
50	34.54	0.17
70	32.79	4.29
100	19.94	21.03
140	8.81	25.52
200	2.23	19.59
270	0.33	15.50
pan	0.01	13.90
Total	100.00	100.00
AFS GFN	57	143

Table 4. Sieve analysis and AFS grain fineness number for ViriCast™ powder

ASTM E-11 Sieve Size	Percent Retained
30	1.12
40	0.38
50	0.15
70	0.16
100	1.17
140	7.22
200	26.99
270	18.55
Pan	44.26
TOTAL	100.00
AFS GFN	216

The particle size distribution data may involve some error due to the particles of the ViriCast™ powder clinging to the sieves by static electricity. Regardless, the sieve analysis demonstrated that the ViriCast™ powder is significantly finer than the ZCast® powder, and both 3DP powders are much smaller in size than the no-bake sand.

Tensile Testing

Dog bone shaped specimens were produced from the mold materials and tested following the experimental plan (Section 2.1). The results of tensile testing are reported in Table 5.

Table 5. Tensile strengths of the different mold materials

Mold Material	Mean σ (MPa)	SD (MPa)	Wilcoxon Comparison <i>p</i>-Value	
No-Bake	0.56	0.09	X	-----
ViriCast™	0.16	0.03	0.0081	X
ZCast®	0.06	0.02	0.0369	0.0282

Statistical software (JMP 10.0.2) was used to investigate potential significant difference in the tensile strengths of the two printed mold materials. Non-parametric Wilcoxon tests were performed on the data using a level of significance (α) of 0.05 after confirming the data was not normal. The *p*-values from the comparisons are displayed in Table 5. The no-bake molds were significantly stronger than the two 3DP materials. Additionally, the ViriCast™ material was significantly stronger than the ZCast®. While ViriCast™ was weaker than the traditional no-bake foundry sand, it would make a more durable and handleable mold than the ZCast® 3DP powder.

3.2. Properties of Cast A356 Cylinders

Cylindrical specimens cast from the two 3DP mold materials were compared to sand casted A356-T6 alloy cylinders of the same size. The metal specimens cast in no-bake molds were prepared using a different A356 melt than the metal samples cast using 3DP molds. The same T6 heat treatment was performed on the metal specimens produced with both the 3DP and no-bake sand molds. Compositional analysis performed on the two different melts using a Bruker Q4 Tasman Advanced CCD-Based Optical Emission Spectrometer showed that both melts were in the range of standard A356 alloy chemistry values.

Surface Roughness

The results of the surface roughness testing are reported in Table 6. After confirming the data followed a normal distribution, a student's t-Test with a level of significance (α) of 0.05 was used to determine if the surface roughnesses of the cylindrical specimens cast using different mold materials were significantly different.

Table 6. Surface roughness average (Ra) measurements of the overall metal specimens

Mold Material	Mean (μm)	SD (μm)	T-Test Comparison <i>p</i>-Value	
No-Bake	12.17	2.87	X	-----
ViriCast™	13.62	3.11	0.1223	X
ZCast®	15.62	2.85	0.0002	0.0559

Specimens prepared using ZCast® molds had the roughest surface finish on average. The samples produced using no-bake molds were significantly smoother than those cast from ZCast® but not compared to ViriCast™. Additionally, the ViriCast™ 3DP and ZCast® molds produced significantly equivalent surface roughnesses.

Surface finish is a function of sand particle size and distribution. Fine grain sands tend to produce better surface finishes but reduce the permeability of the mold to gasses [19]. Additionally, previous tests show that ZCast® molds produce a larger amount of gasses during casting due to the binder used during the binder jetting process [2]. The increase in gas in ZCast® molds, in combination with the smaller particle size in both 3D powders, could explain the larger surface roughness in ZCast® and ViriCast™, although significantly greater in ZCast® castings.

Sand casting processes typically produce cast parts with surface roughness values between 12.5 and 25 μm [20]. Although specimens produced using the 3DP molds had a rougher surface finish than the no-bake specimens, their surface roughness values still fall on the low range of typical sand cast surface roughness values [20].

Density

The average densities of cylindrical specimens of A356-T6 aluminum cast from different mold materials are reported in Table 7. The densities of the specimens cast from 3DP molds were less than the standard density for the A356-T6 alloy (2.66-2.71 g/cm^3) [21]. The sample densities were lower than expected due to porosity observed throughout the cast pieces. The overall density data for the specimens did not have a normal distribution; as a result a non-parametric Wilcoxon test ($\alpha = 0.05$) was used for statistical comparison. The average density of no-bake and ViriCast™ castings didn't vary significantly as well as between ViriCast™ and ZCast®. On the other hand, the densities of ZCast® castings did vary significantly from no-bake castings. This could be due to larger percentage of porosity in the ZCast® castings. The density did not vary significantly throughout the length of the specimens regardless of the mold material.

Table 7. Average density measurements of overall metal specimens (mean values and SD)

Mold Material	Mean (g/cm ³)	SD (g/cm ³)	Wilcoxon Comparison	
			<i>p</i> -Value	
No-Bake	2.61	0.05	X	-----
ViriCast™	2.61	0.02	0.1497	X
ZCast®	2.59	0.04	0.0175	0.1837

Porosity

The amount of porosity present in the specimens was determined by analyzing micrographs of the polished aluminum samples. Micrographs demonstrating the porosity of metal cast using the three different mold materials are shown in Figure 4. The average porosity values for the entire samples are reported in Table 8. After determining the data was not normal, a non-parametric Wilcoxon test ($\alpha = 0.05$) was used to determine if differences in the data were significantly different.

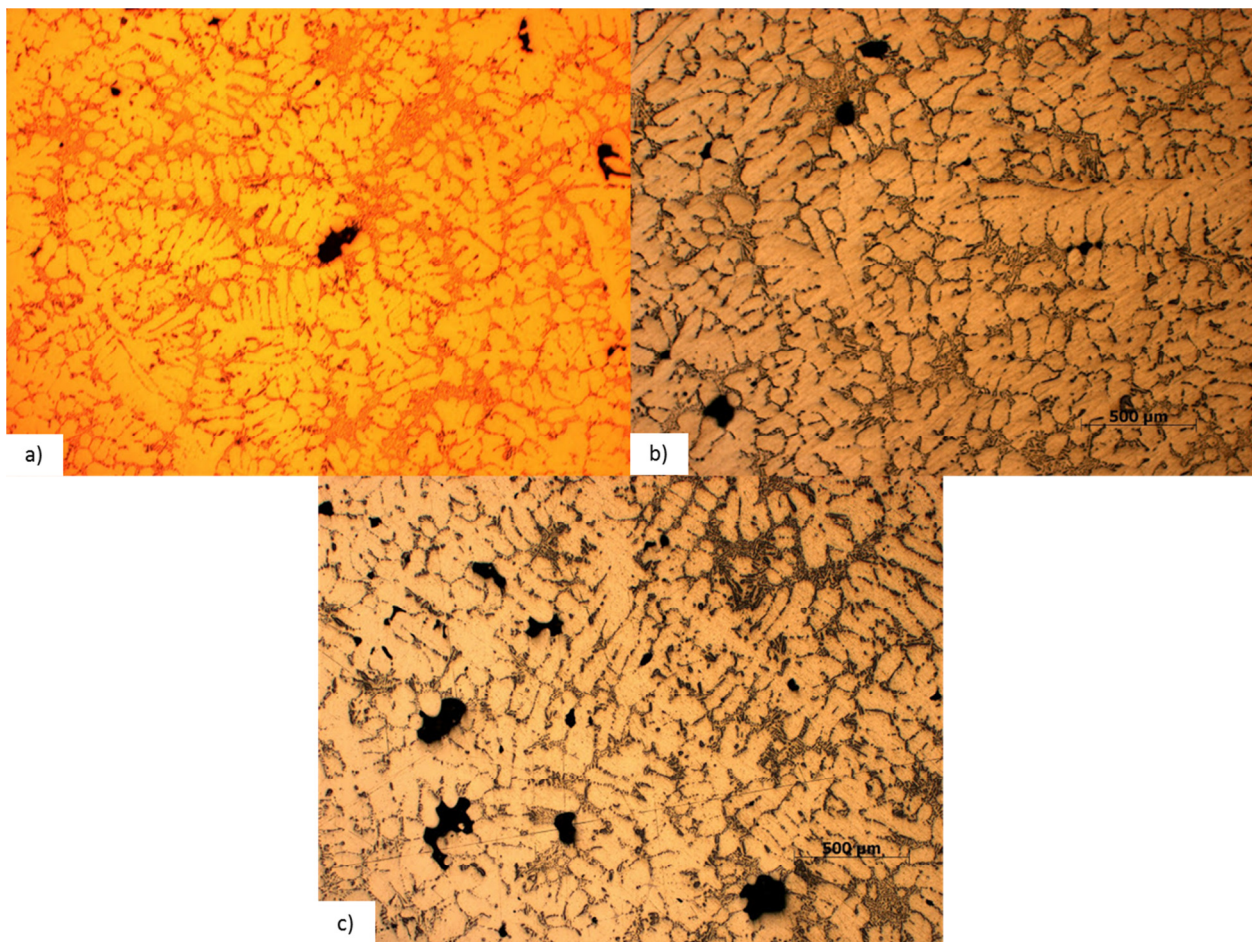


Figure 4. Micrographs of T6-A356 aluminum cast in traditional no-bake (a), ViriCast™ (b), and ZCast® (c) molds

Table 8. Average porosity values of overall metal specimens (mean values and SD)

Mold Material	Mean (%)	SD (%)	Wilcoxon Comparison <i>p</i>-Value	
No-Bake	0.65	0.53	X	-----
ViriCast™	1.13	0.71	<0.0001	X
ZCast®	1.59	1.36	<0.0001	0.1445

The porosity observed in samples cast in ZCast® molds was higher than the samples cast in ViriCast™ molds, but not significantly. Porosity in the samples cast in ZCast® molds had a large standard deviation in relation to the average. The porosity seen in specimens prepared with no-bake molds was significantly less than the cylinders prepared using 3DP molds. This is most likely due to the higher binder content of 3DP molds. During the pouring process, off-gassing of the binder causes entrapped gasses that lead to porosity in the final cast parts.

During the cylinder sectioning process, the orientations of the middle sections were not kept consistent. So, data from the middle sections may represent data taken from Faces 1 or 2 (see Figure 3b). The top data points were all taken at Face 1, and the bottom data points were either taken at Face 2 or Face 3. As a result, the data from the middle section does not provide useful information for comparison. The data from the top and bottom sections still can be used to analyze trends in metals properties throughout the length of the mold.

Analysis of the top and bottom sections showed that porosity did not vary significantly throughout the length of the cylindrical samples cast in 3DP molds, as shown in Figure 5. The standard deviation was so large in both locations that even though there appears to be a trend in the means, the differences were not statistically significant. In the no-bake molds, the metal at the bottom of the mold was significantly more porous than the metal at the top of the mold.

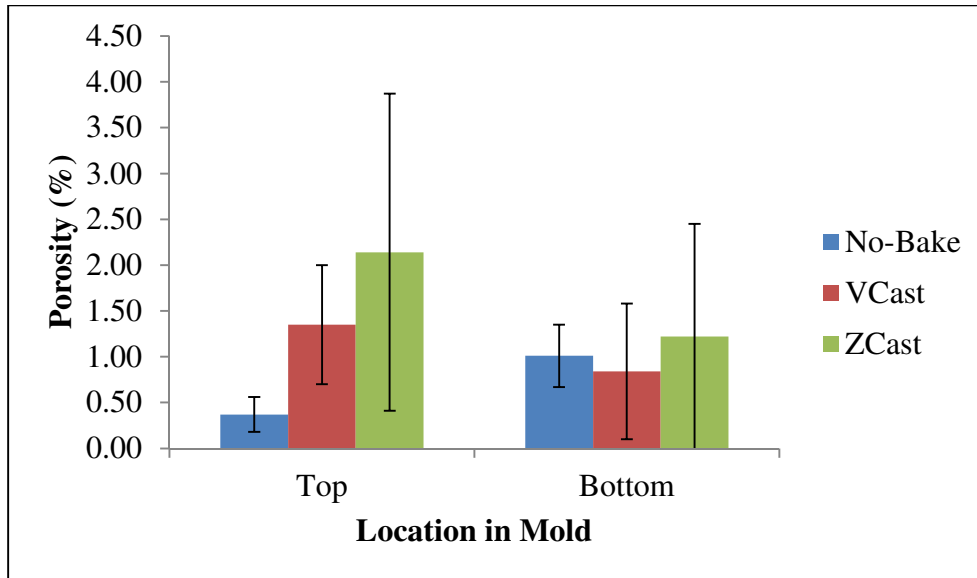


Figure 5. Variation of porosity of cast A356-T6 throughout the length of the mold

Microstructure

After etching the polished aluminum samples, the dendrite arm spacing was measured using optical microscopy. Statistical analysis was performed on the data using a non-parametric Wilcoxon test ($\alpha = 0.05$). The results of the microscopy measurements are shown in Table 9. Micrographs displaying representatives of the A356 microstructure from each mold type are shown in Figure 6. The microstructure was analyzed to determine if the different melts provided like mechanical properties for the aluminum cylinders. Finer dendrite arm spacing is desirable for better mechanical property performance. The larger the dendrite arm spacing, the coarser the microconstituents and the more prominent their effects on properties [22].

Table 9. Average dendrite arm spacing in the overall metal specimens

Mold Material	Mean (μm)	SD (μm)	Wilcoxon Comparison p -Value	
No-Bake	41.2	5.32	X	-----
ViriCast™	72.0	9.74	<0.0001	X
ZCast®	72.9	7.28	<0.0001	0.7559

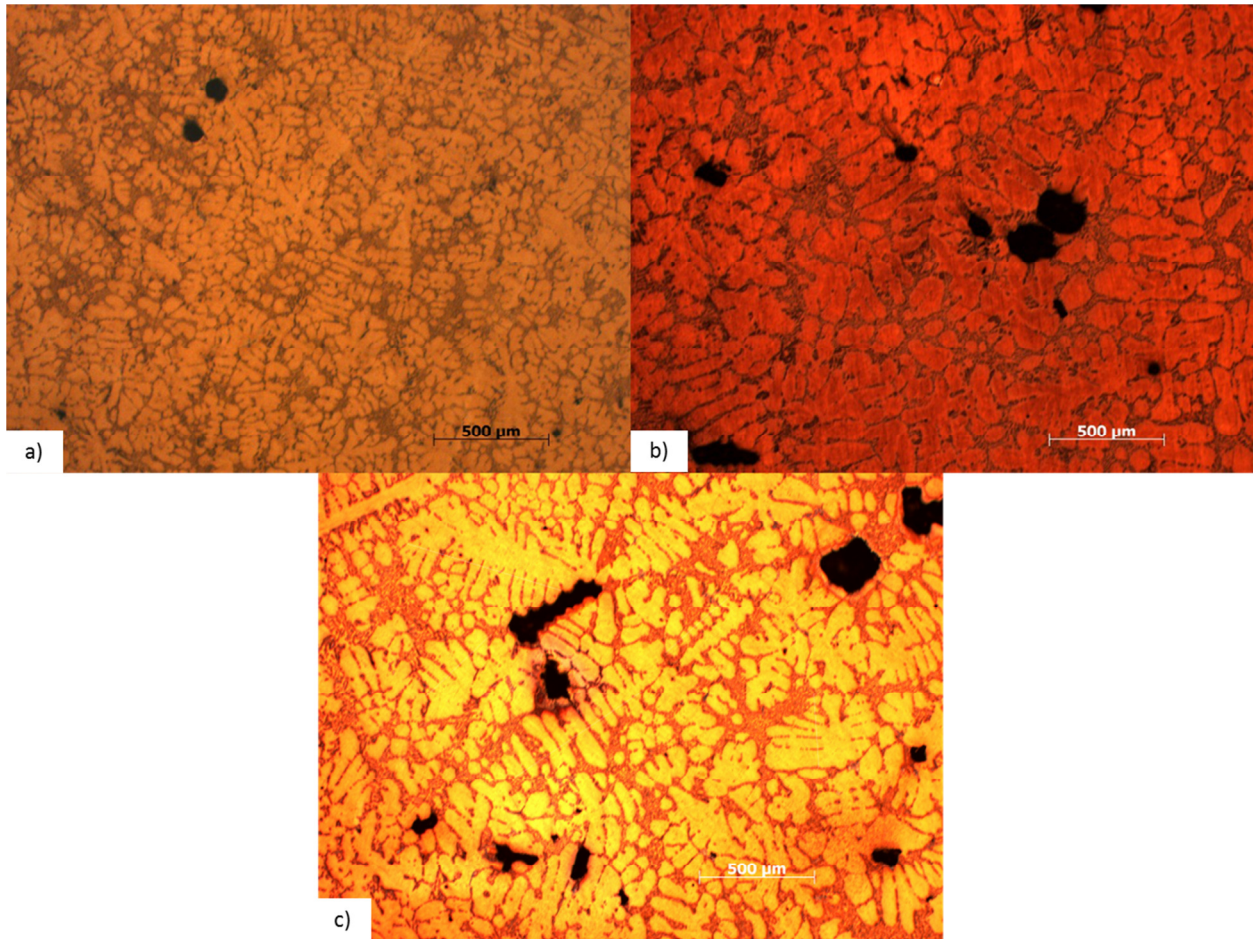


Figure 6. Dendritic microstructure of A356-T6 alloy cast in no-bake a), ViriCast™ b), and ZCast® c) molds

The dendrite arm spacing in the samples cast in ZCast® and ViriCast™ molds were not significantly different. The samples prepared using no-bake molds had significantly smaller dendrite arm spacing than the 3DP prepared specimens. This indicates the heat treating processes varied between the two 3DP pieces and the no-bake parts. The T6 heat treatment was performed on all the specimens cast in 3DP molds at the same time, but the heat treatment on the samples cast in no-bake molds was completed at a different time and in another furnace. Since the heat treatments differed, the mechanical properties (hardness and compressive yield strength) of the no-bake specimens cannot be compared to those of the 3DP prepared metal cylinders. Heat treating does not affect the porosity, surface roughness, or density of the aluminum specimens, thus valid comparisons can still be made between the no-bake cylinders and 3DP cylinders for the above tests [22].

Hardness

The Vickers Hardness values of the cylindrical specimens were measured and used to compare the metals cast from different mold materials. After determining the data was not

normal, a non-parametric Wilcoxon test ($\alpha = 0.05$) was used to determine if differences in the data were significantly different. The results of the hardness testing are reported in Table 10.

Table 10. Vickers hardness values of the overall metal specimens

Mold Material	Mean (HV)	SD (HV)	Wilcoxon Comparison <i>p</i>-Value	
No-Bake	82.1	4.83	X	-----
ViriCast™	92.7	9.67	<0.0001	X
ZCast®	94.3	9.60	<0.0001	0.6204

The Vickers hardness values for specimens produced using ViriCast™ and ZCast® molds did not vary significantly from each other. The test values for both specimens produced using 3DP molds fell within the normal hardness value range of 87.38 – 96.65 HV for the A356-T6 alloy [21]. The hardness values did not vary significantly throughout the length of the cast cylindrical specimens. The specimens produced by both the 3DP printed molds were significantly harder than the samples produced using traditional no-bake molds. The differences observed in hardness between the specimens produced with no-bake and 3DP molds are most likely due to an issue with heat treating the no-bake specimens, as mentioned previously. In all of the mold types, hardness values did not vary significantly with mold location. The metal in the top and bottoms of the molds had statistically equivalent hardness values.

Compression Testing

Metal cylinders produced from the 3DP molds were machined to match compression specimen requirements [15]. Compressive yield strengths were determined and compared against published values to determine if the 3DP molds produced cast samples with mechanical properties comparable to traditional foundry techniques. A Wilcoxon test ($\alpha = 0.05$) was used to determine if there were any significant yield strength differences between castings from no-bake, ZCast®, and ViriCast™ molds. The results of the compression testing are shown in Table 11. An example stress-strain curve for a cylinder cast using a ZCast® mold is shown in Figure 7.

Table 11. Compression testing of cast A356-T6 alloy species. No-bake compressive yield strengths were obtained from published sources [14].

Mold Material	Mean Compressive Yield Strength, σ (MPa)	SD (MPa)	Wilcoxon Comparison p -Value
No-Bake	165-195 [22–24]		-----
ViriCast™	170.8	30.5	X
ZCast®	180.8	35.8	0.2971

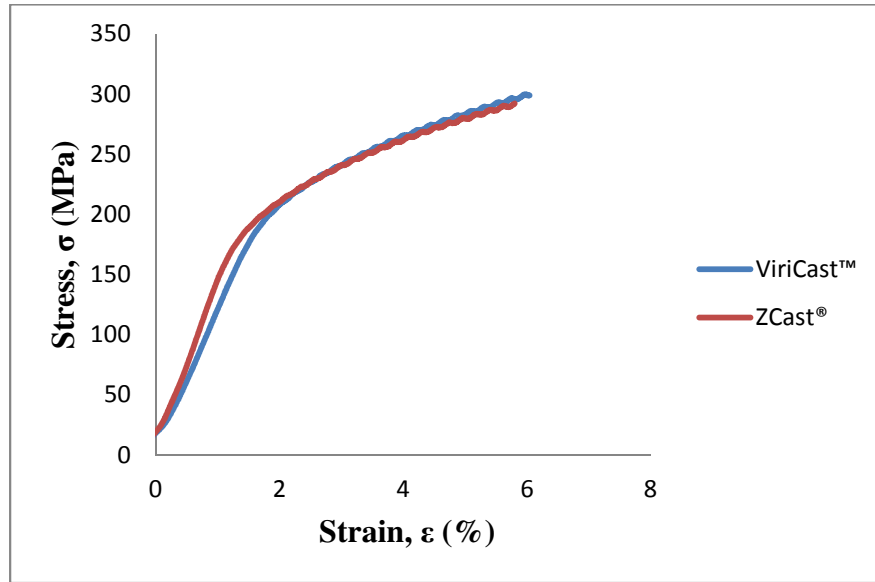


Figure 7. Compressive stress-strain curve for A356-T6 cylinders cast in ZCast® and ViriCast™ molds

The compressive yield strengths of the specimens cast using 3DP molds fell within the range of published data. This shows that metal parts produced using additive manufacturing techniques have the same mechanical properties in compression as those produced using traditional sand casting techniques. The yield strengths of the cast metal did not vary significantly between the two 3DP mold materials ($p=0.2971$).

4. CONCLUSIONS AND FUTURE WORK

The binder jetting 3DP process has been used to produce molds to cast complex structures. In this work, two 3DP powders, ViriCast™ and ZCast®, were compared on the basis of handleability of the printed molds and quality of the cast metal they produced. The two 3DP powders yielded nearly identical samples. Samples cast using ViriCast™ and ZCast® molds were statistically equivalent on all six tests performed.

Additionally, the handleability and metal casting abilities of the 3DP powders were compared to traditional no-bake foundry sand molds. It was determined that the binder jetting process can be used to produce metal specimens with similar properties to those created using

traditional sand casting techniques. Both the ViriCast™ and ZCast® 3DP molds produced cast metal parts with the same mechanical performance and hardness as traditionally prepared A356-T6. However, ZCast® molds produced cast A356-T6 with greater surface roughness and decreased density than the samples prepared with no-bake molds. Furthermore, the no-bake molds had a significantly higher tensile strength than the 3DP molds, which made them more handleable, while produced castings with less porosity and smaller dendrite arm spacing.

As technology advances, modeling, including flow modeling and solidification, will yield higher quality castings by minimizing porosity resulting in desired microstructure. Due to the freedom of design provided by Additive Manufacturing, the molder has the ability to overcome the manufacturing constraints of traditional mold making in order to generate optimal complex castings. Continued work with these molding materials, in addition to others, will provide the ability to enhance existing lightweight, stiff cellular structures with designed mesostructure [6].

REFERENCES

- [1] P. R. Beely, *Foundry Technology*. Butterworth-Heinemann, 2001.
- [2] D. A. Snelling, V. Tech, R. Kay, A. Druschitz, and C. B. Williams, "Mitigating Gas Defects in Castings Produced from 3D Printed Molds," in *117th Metalcasting Congress*, 2012.
- [3] 3D Systems, "Solutions: Metal Casting." [Online]. Available: <http://www.zcorp.com/en/Solutions/Castings-Patterns-Molds/spage.aspx>.
- [4] ExOne, "ExOne: Digital Part Materialization." [Online]. Available: <http://www.exone.com/materialization/what-is-digital-part-materialization/sand>.
- [5] Viridis3D, "Metal Casting." [Online]. Available: <http://www.viridis3d.com/metalcasting.htm>.
- [6] N. A. Meisel, C. B. Williams, and A. Druschitz, "Lightweight Metal Cellular Structures via Indirect 3D Printing and Casting," in *SFF Symposium*, 2012.
- [7] J. Campbell, *Castings*, 2nd ed. Butterworth-Heinemann Limited, 2003.
- [8] M. Chhabra and R. Singh, "Obtaining desired surface roughness of castings produced using ZCast direct metal casting process through Taguchi's experimental approach," *Rapid Prototyping Journal*, vol. 18, pp. 458–471, 2012.
- [9] E. Bassoli, A. Gatto, L. Iuliano, and M. G. Violante, "3D printing technique applied to rapid casting," *Rapid Prototyping Journal*, vol. 13, no. 3, pp. 148–155, 2007.
- [10] S. S. Gill and M. Kaplas, "Efficacy of powder-based three-dimensional printing (3DP) technologies for rapid casting of light alloys," *The International Journal of Advanced Manufacturing Technology*, vol. 52, no. 1–4, pp. 53–64, May 2010.
- [11] N. Mckenna, S. Singamneni, O. Diegel, D. Singh, T. Neitzert, J. S. George, A. R. Choudhury, and P. Yarlagadda, "QUT Digital Repository : Direct Metal casting through 3D printing : A critical analysis of the mould characteristics," in *Global Congress on Manufacturing and Management*, 2008, pp. 12–14.
- [12] S. S. Gill and M. Kaplas, "Comparative Study of 3D Printing Technologies for Rapid Casting of Aluminium Alloy," *Materials and Manufacturing Processes*, vol. 24, no. 12, pp. 1405–1411, Dec. 2009.
- [13] American Foundry Society, *Mold and Core Test Handbook*, 3rd ed. Des Plaines: American Foundry Society, 2004.

- [14] ASM International, *Metals Handbook: Properties and Selection: Nonferrous Alloys and Pure Metals*, 10th ed., vol. 2. ASM International, 1990.
- [15] ASTM International, *Standard Test Methods of Compression Testing of Metallic Materials at Room Temperature*. ASTM Standard E9-09, 2009.
- [16] National Institutes of Health, “ImageJ: Image Processing and Analysis in Java.” [Online]. Available: <http://rsb.info.nih.gov/ij>.
- [17] G. Vander Voort, “Metallography and Microstructure of Aluminum and Alloys.” [Online]. Available: <http://www.vacaero.com/Metallography-with-George-Vander-Voort/Metallography-with-George-Vander-Voort/metallography-and-microstructure-of-aluminum-and-alloys.html>.
- [18] G. Vander Voort, “Metallographic Etching of Aluminum and its Alloys.” [Online]. Available: http://www.georgevandervoort.com/met_papers/Aluminum/AIEtchExperiment.pdf.
- [19] U. C. Nwaogu and N. S. Tiedje, “Foundry Coating Technology: A Review,” *Materials Sciences and Applications*, vol. 02, no. 08, pp. 1143–1160, 2011.
- [20] L. J. Star Inc., “Surface Finish Charts.” [Online]. Available: http://www.ljstar.com/design/surface_charts.aspx.
- [21] Granta Design Limited, “CES EduPack.” 2013.
- [22] J. G. Kaufman and E. L. Rooy, *Aluminum Alloy Castings: Properties, Processes, and Application*. ASM International, 2004.
- [23] MatWeb, “MatWeb: Material Property Data.” [Online]. Available: <http://www.matweb.com>.
- [24] J. R. Davies, *Aluminum and Aluminum Alloys*. ASM International, 1993.